Thermal Boundary Resistance Measurements for Phase-Change Memory Devices

John P. Reifenberg, Kuo-Wei Chang, Matthew A. Panzer, Sangbum Kim, Jeremy A. Rowlette, Mehdi Asheghi, H.-S. Philip Wong, and Kenneth E. Goodson

***Abstract*—Thermal interfaces play a key role in determining the programming energy of phase-change memory (PCM) devices. This letter reports the picosecond thermoreflectance measurements of thermal boundary resistance (TBR) at TiN/GST and Al/TiN interfaces, as well as the intrinsic thermal conductivity measurements of fcc GST between 30 °C and 325 °C. The TiN/GST TBR decreases with temperature from ∼26 to ∼18 $m^2 \cdot K/GW$, and the Al/TiN ranges from ∼7 to 2.4 $m^2 \cdot K/GW$. A TBR of 10 $m^2 \cdot K/GW$ is equivalent in thermal resistance to ∼192 nm of TiN. The fcc GST conductivity increases with temperature between ∼0.44 and 0.59 W/m/K. A detailed understanding of TBR is essential for optimizing the PCM technology.**

***Index Terms*—Nonvolatile memories, phase-change memory (PCM), thermal boundary resistance (TBR).**

I. Introduction

PHASE-CHANGE memory (PCM) data storage technology offers the scalability, cycling characteristics, and speed to meet the ever-increasing demand for high-density data storage. Joule heating initiates reversible phase transitions between the amorphous and fcc phases of a phase-change material such as $Ge_2Sb_2Te_5$ (GST) [1], [2]. The GST temperature reaches up to 700 °C during the phase transitions [3]. Write current reduction remains a challenge for decreasing the size of programming transistors. Programming pulses contain ∼1000 times more energy than what is required for the phase transitions. Heat conduction through the bottom electrode, commonly made of TiN, dissipates most of the excess energy [3], [4]. Understanding the conduction physics in thin TiN and GST films and at their interfaces is therefore essential for improved PCM device engineering and simulation [3], [5], [6]. This letter uses picosecond time-domain thermoreflectance (TDTR) [7], [8] to measure the fcc GST intrinsic thermal conductivity and the TiN/GST and Al/TiN thermal boundary resistances (TBRs) between room temperature and 325 °C.

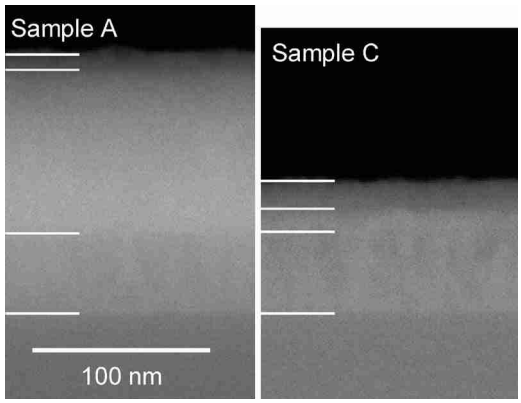

Fig. 1. Cross-sectional SEM images of two measured samples. From the top, the layers are TiN, fcc GST, TiN, and Si. Approximately 53-nm layers of Al were evaporated on these structures and measured using AFM after the SEMs were taken. The white lines are intended as a guide for distinguishing between layers.

II. Picosecond Thermoreflectance Measurement

Picosecond TDTR is a well-established technique [7]–[9] that measures the cross-plane distribution of thermal properties with deep submicrometer spatial resolution. Other thermal metrology techniques such as nanosecond thermoreflectance [10] and 3ω[11] resolve spatially averaged thermal properties, typically providing only indirect measurements of TBR. In contrast, picosecond TDTR can uniquely separate the TBR from intrinsic thermal resistance.

A mode-locked Nd:YVO_4 laser produces ∼9-ps pulses at wavelength $\lambda = 1064$ nm with a repetition rate of 82 MHz. The beam splits into a frequency-doubled pump beam modulated at 8 MHz, which heats the surface of a metal-coated sample. The reflected intensity of the probe beam measures the surface temperature decay with ∼9-ps temporal resolution over a temporal range of 3.5 ns [7], [8]. The 19-mW 10.0-μm $1/e^2$-diameter pump and 10-mW 5.0-μm $1/e^2$-diameter probe beams cause instantaneous and steady temperature rises of less than 6 °C and 1.5 °C, respectively, for a reflectance of ∼0.9 [9].

Four TiN/GST/TiN stacks were produced by physical vapor deposition (PVD) on Si substrates at 135 °C. Fig. 1 shows the scanning electron microscope (SEM) images of two of the TiN/GST/TiN stacks. Table I lists the sample geometries. TDTR requires the top metal to be opaque at the pump and probe wavelengths; thus, ∼53 nm of Al was evaporated on

Manuscript received September 22, 2009; revised October 14, 2009. First published November 17, 2009; current version published December 23, 2009. This work was supported in part by Intel Corporation and in part by a National Defense Science and Engineering Graduate Fellowship. The review of this letter was arranged by Editor A. Chatterjee.

J. P. Reifenberg, M. A. Panzer, M. Asheghi, and K. E. Goodson are with the Department of Mechanical Engineering, Stanford University, Stanford, CA 94305 USA (e-mail: jreif@stanford.edu; mpanzer@stanford.edu; masheghi@stanford.edu; goodson@stanford.edu).

K.-W. Chang is with Intel Corporation, Santa Clara, CA 95054 USA (e-mail: kuo-wei.chang@intel.com).

S. Kim, J. A. Rowlette, and H.-S. P. Wong are with the Department of Electrical Engineering, Stanford University, Stanford, CA 94305 USA (e-mail: kimsangb@stanford.edu; rowlette@stanford.edu; hspwong@stanford.edu).

Color versions of one or more of the figures in this letter are available online at http://ieeexplore.ieee.org.

Digital Object Identifier 10.1109/LED.2009.2035139

TABLE I
THIN-FILM GEOMETRIES FOR DIFFERENT SAMPLES. THE SAMPLE GEOMETRY IS Al/TOP, TiN/GST/BOTTOM, AND TiN/Si SUBSTRATE

	Aluminum	Top TiN Layer	GST	Bottom TiN Layer
Sample A	52.5 nm	10.8 nm	91.4 nm	45.1 nm
Sample B	52.5 nm	10.3 nm	51.9 nm	47.3 nm
Sample C	52.5 nm	15.7 nm	14.0 nm	44.5 nm
Sample D	52.5 nm	17.4 nm	6.5 nm	47.4 nm

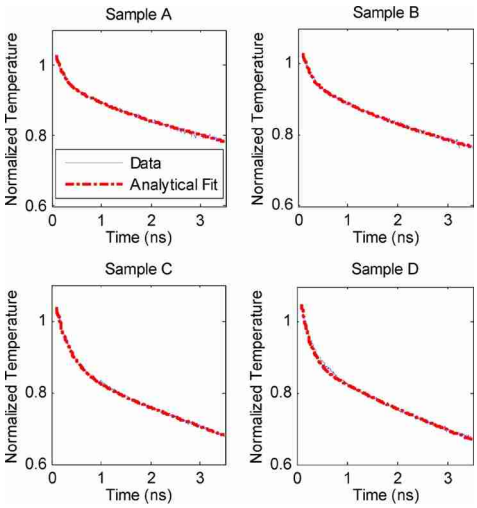

Fig. 2. Representative thermal traces and data fits at 30 °C for each of the four samples. Each thermal decay trace is the average of ten traces.

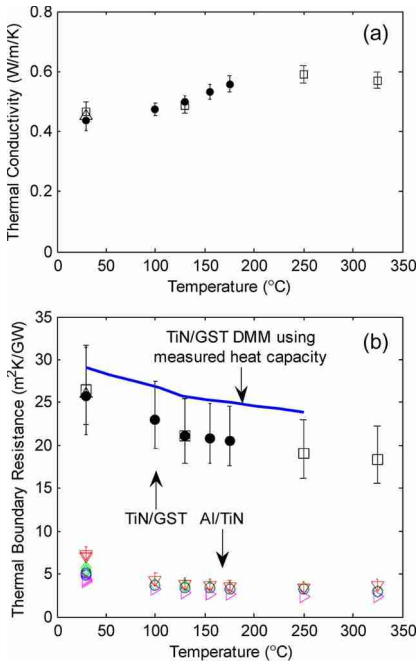

Fig. 3. (a) GST intrinsic thermal conductivity and (b) TiN/GST and Al/TiN TBRs. For the GST intrinsic conductivity and TiN/GST TBR, ● indicates measurements from the initial temperature ramp between 30 °C to 175 °C, □ indicates measurements after ramping back to 30 °C then up to 325 °C, and △ indicates the final measurement after ramping back to 30 °C. The ◯, ◊, ▽, and ▷ indicate the Al/TiN TBRs for samples A, B, C, and D, respectively. For clarity, error bars are shown only for sample C. Al/TiN TBR errors are similar for other samples.

the exposed TiN surface after an extended air break. Atomic force microscopy (AFM) measurements over a masked region determine the Al thicknesses. The thickness uncertainties are ±2.5 nm for the Al films and ±1.5 nm for the TiN and GST films.

A transient 3-D multilayer frequency domain solution to the heat diffusion equation [9] models the measured thermal decays. A nonlinear least squares curve fitting algorithm finds the TiN/GST TBR, Al/TiN TBRs, and intrinsic GST conductivity that simultaneously optimize the curve fits for all four samples. Data are fit using GST heat capacity data from [12]. Fig. 2 shows the representative data and curve fits for each sample from the final measurement at 30 °C. The fits are insensitive to the initial guess. To reduce the influence of random noise, we average ten traces for each sample at every temperature and normalize by the average value between 100 and 115 ps. Data are fit over the range 100–3500 ps.

The metal's thermal diffusion time τ due to the Al/TiN boundary is $\tau \sim R_{b,\mathrm{Al/TiN}}C$, where $R_{b,\mathrm{Al/TiN}}$ is the Al/TiN TBR and C is the thermal mass of the Al layer. At times less than $\tau \sim 650$ ps, the thermal decay is highly sensitive to the Al/TiN TBR and minimally sensitive to other thermal properties. This permits unique fitting of the Al/TiN TBR in each sample.

At long times $t > 2000$ ps, the influence of the Al/TiN resistance is small compared to the underlying films' thermal impedances. The sample geometry determines the relative sensitivities to the TiN/GST TBR and intrinsic thermal conductivity. For example, the intrinsic GST conductivity dominates the response of sample A since heat does not diffuse entirely through the GST film during the measurement time range. Sample D has sensitivity to both the TiN/GST TBR and intrinsic thermal conductivity since heat diffuses through the entire stack. The unique extraction of the TiN/GST TBR is possible under the assumption that the intrinsic GST conductivity and TiN/GST TBR are the same in all samples.

III. RESULTS AND DISCUSSION

Fig. 3 shows the fitted Al/TiN, GST/TiN, and intrinsic GST thermal conductivity as a function of temperature between 30 °C and 325 °C. The Al films cracked, and the GST films sublimated near 350 °C, preventing measurements at higher temperatures. Other metals, such as W, also cracked at high temperature and exhibited smaller signal-to-noise ratios and nonthermal responses at short times, similar to those in [13]. The measurement time at each temperature was 30 ±5 min. The intrinsic GST thermal conductivity values between 0.44 and 0.59 W/m/K agree well with previous fcc phase measurements [10], [11], [14], [15]. The glasslike temperature dependence of the thermal conductivity is likely due to the large vacancy and interstitial concentration in fcc GST [14]. The data do not show hysteresis with annealing, suggesting that irreversible changes in defect density are not significant in our films, in contrast to [14]. This may be due to the higher deposition temperature of our films. The TiN/GST TBR varies between ∼26 and 18 $\mathrm{m}^2 \cdot \mathrm{K/GW}$. A TBR of 10 $\mathrm{m}^2 \cdot \mathrm{K/GW}$ is approximately equivalent in thermal resistance to 192 nm of TiN. The Al/TiN TBR varies between ∼7 and 2.3 $\mathrm{m}^2 \cdot \mathrm{K/GW}$.

Different levels of oxidation, contamination, and roughness explain the difference in Al/TiN values between samples.

We use nanosecond transient thermoreflectance [10] to measure the room temperature effective thermal conductivity $k_{\rm eff}$ of $\sim$60-, 100-, and 120-nm layers of PVD TiN on Si, coated with $\sim$500-nm PVD Ti. By modeling the data as thermal resistors in series [11], the relation $1/k_{\rm eff} = 1/k_{\rm int,TiN} + 2R_{b,\rm avg}/d$ determines the intrinsic TiN conductivity $k_{\rm int} = 19.2$ W/m/K and the average of the Ti/TiN and TiN/Si TBRs $R_{b,\rm avg} = 11.8$ m^{2}K/GW, where d is the TiN layer thickness. The error bars in Fig. 3 account for the thickness uncertainties, $\pm$50% variation in $k_{\rm int,TiN}$ [16], and TiN/Si TBRs between 0 and 11.8 m$^2 \cdot$ K/GW.

Phonons dominate thermal transport in fcc GST [14] and high-resistivity PVD TiN films. The acoustic mismatch (AMM) and diffuse mismatch (DMM) models describe TBR as the partial transmission of phonons across an interface [15]. While many variations of these models exist [18], the DMM using the measured heat capacity

$$R_b = \left(\frac{\sum_j c_{2,j}^{-2}}{12\left(\sum_j c_{1,j}^{-2} + \sum_j c_{2,j}^{-2}\right)} \sum_j c_{1,j} \right)^{-1} C_1(T)^{-1} \qquad (1)$$

best represents the data, where R_b is the TBR, $C_1(T)$ is the measured heat capacity of material 1 at temperature T, and $c_{i,j}$ is the velocity of phonon mode j in material i [18]. Fig. 3 shows that this model overpredicts the data but captures its temperature trend. It estimates the Al/TiN TBR as $\sim$0.3 m$^2 \cdot$ K/GW at 30 °C. The large disagreement between the model and the measured value of the Al/TiN TBR is likely due to impurity adsorption and oxidation during the air break between Al evaporation and the initial deposition. Materials with dissimilar Debye temperatures (i.e., large AMM) have larger TBRs, which explains the difference in the TiN/GST and Al/TiN TBRs. Acoustically mismatched phase-change and electrode materials should therefore provide better thermal insulation of the PCM programming region. The Debye temperature of fcc GST is $\sim$100 K [19], while the Debye temperature of TiN is $\sim$557 K [20]. Stiff materials with low density such as carbon nanotubes have the highest Debye temperatures, up to $\sim$2000 K [21].

The AMM and DMM predict constant TiN/GST TBR at device operating temperatures. The data show decreasing TBR with temperature for both TiN/GST and Al/TiN interfaces. Lattice dynamics calculations on Lennard–Jones solids predict decreasing TBR up to the melting point [22]. A recent experimental work attributes a $1/T$ dependence of the TBR to anharmonic phonon processes [13]. Assuming a $1/T$ temperature dependence coincident with the data at 325 °C, the TiN/GST TBR extrapolates to $\sim$12.6 m$^2 \cdot$ K/GW at the GST melting temperature of 610 °C.

IV. Conclusion

This letter has been using an original multisample data extraction technique in the first temperature-dependent measurements of the TiN/GST TBR, which are critical quantities for PCM device simulations and engineering. DMM calculations using the measured heat capacity have offered the best simple means to estimate the TBR between electrode and phase-change materials. Acoustically mismatched phase-change and electrode materials may improve the thermal isolation of the PCM programming region.

References

[1] S. Lai, "Current status of phase change memory and its future," in *IEDM Tech. Dig.*, 2003, pp. 255–258.

[2] A. L. Lacaita, "Phase change memories: State-of-the-art, challenges, and perspectives," *Solid State Electron.*, vol. 50, no. 1, pp. 24–31, Jan. 2006.

[3] J. P. Reifenberg, D. L. Kencke, and K. E. Goodson, "The impact of thermal boundary resistance in phase-change memory devices," *IEEE Electron Device Lett.*, vol. 29, no. 10, pp. 1112–1114, Oct. 2008.

[4] S. M. Sadeghipour, L. Pileggi, and M. Asheghi, "Phase change random access memory, thermal analysis," in *Proc. ITHERM*, 2006, pp. 660–665.

[5] D. L. Kencke, I. V. Karpov, B. G. Johnson, S. J. Lee, D. Kau, S. J. Hudgens, J. P. Reifenberg, S. D. Savransky, J. Zhang, M. D. Giles, and G. Spadini, "The role of interfaces in damascene phase change memory," in *IEDM Tech. Dig.*, 2007, pp. 323–326.

[6] C. Kim, D.-S. Suh, K. H. P. Kim, Y.-S. Kang, T.-Y. Lee, Y. Khang, and D. G. Cahill, "Fullerene thermal insulation for phase change memory," *Appl. Phys. Lett.*, vol. 92, no. 1, p. 013 109, Jan. 2008.

[7] M. A. Panzer, M. Shandalov, J. A. Rowlette, Y. Oshima, Y. W. Chen, P. C. McIntyre, and K. E. Goodson, "Thermal properties of ultra-thin hafnium oxide gate dielectric films," *IEEE Electron Device Lett.*, vol. 30, no. 12, pp. 1269–1271, Dec. 2009.

[8] J. Rowlette, R. Kekatpure, M. Panzer, M. Brongersma, and K. Goodson, "Nonradiative recombination in strongly interacting silicon nanocrystals embedded in amorphous silicon-oxide films," *Phys. Rev. B, Condens. Matter*, vol. 80, no. 4, p. 045 314, Jul. 2009.

[9] D. G. Cahill, "Analysis of heat flow in layered structures for time-domain thermoreflectance," *Rev. Sci. Instrum.*, vol. 75, no. 12, pp. 5119–5122, Dec. 2004.

[10] J. P. Reifenberg, M. A. Panzer, S. Kim, A. M. Gibby, Y. Zhang, S. Wong, H.-S. P. Wong, E. Pop, and K. E. Goodson, "Thickness and stoichiometry dependence of the thermal conductivity of GeSbTe films," *Appl. Phys. Lett.*, vol. 91, no. 11, p. 111 904, Sep. 2007.

[11] E. K. Kim, S. I. Kwun, S. M. Lee, H. Seo, and J. G. Yoon, "Thermal boundary resistance at $Ge_2Sb_2Te_5/ZnS{:}SiO_2$ interface," *Appl. Phys. Lett.*, vol. 76, no. 26, pp. 3864–3866, Jun. 2000.

[12] J. A. Kalb, "Stresses, viscous flow and crystallization kinetics in thin films of amorphous chalcogenides used for optical data storage," M.S. thesis, Dept. Phys., Univ. Aachen, Aachen, Germany, 2002.

[13] H.-K. Lyeo and D. G. Cahill, "Thermal conductance of interfaces between highly dissimilar materials," *Phys. Rev. B, Condens. Matter*, vol. 73, no. 14, p. 144 301, Apr. 2006.

[14] H.-K. Lyeo, D. G. Cahill, B.-S. Lee, J. R. Abelson, M.-H. Kwon, K.-B. Kim, S. G. Bishop, and B.-K. Cheong, "Thermal conductivity of phase change memory material $Ge_2Sb_2Te_5$," *Appl. Phys. Lett.*, vol. 89, no. 15, p. 151 904, Oct. 2006.

[15] V. Giraud, J. Cluzel, V. Sousa, A. Jacquot, A. Dauscher, B. Lenoir, H. Scherrer, and S. Romer, "Thermal characterization and analysis of phase change random access memory," *J. Appl. Phys.*, vol. 98, no. 1, p. 013 520, Jul. 2005.

[16] T. Vasilos and W. D. Kingery, "Conductivity of some refractory carbides and nitrides," *J. Amer. Ceram. Soc.*, vol. 37, no. 9, pp. 409–414, 1954.

[17] E. T. Swartz and R. O. Pohl, "Thermal boundary resistance," *Rev. Mod. Phys.*, vol. 61, no. 3, pp. 605–668, Jul. 1989.

[18] L. De Bellis, P. E. Phelan, and R. S. Prasher, "Variations of acoustic and diffuse mismatch models in predicting thermal-boundary resistance," *J. Thermophys. Heat Transf.*, vol. 14, no. 2, pp. 144–150, Apr.–Jun. 2000.

[19] T. Blachowicz, M. G. Beghi, G. Guntherodt, B. Beschoten, H. Dieker, and M. Wuttig, "Crystalline phases in the $GeSb_2Te_4$ alloy system: Phase transitions and elastic properties," *J. Appl. Phys.*, vol. 102, no. 9, p. 093 519, Nov. 2007.

[20] P. Patsalas, C. Charitidis, and S. Logothetidis, "The effect of substrate temperature and biasing on the mechanical properties and structure of sputtered titanium nitride thin films," *Surf. Coat. Technol.*, vol. 125, no. 1–3, pp. 335–340, Mar. 2000.

[21] Z. Yao, C. L. Kane, and C. Dekker, "High-field electrical transport in single-wall carbon nanotubes," *Phys. Rev. Lett.*, vol. 84, no. 13, pp. 2941–2944, Mar. 2000.

[22] R. J. Stevens, L. V. Zhigilei, and P. M. Norris, "Effects of temperature and disorder on thermal boundary conductance at solid-solid interfaces: Nonequilibrium molecular dynamics simulations," *Int. J. Heat Mass Transf.*, vol. 50, no. 19/20, pp. 3977–3989, Sep. 2007.